Pergamon

0038-1101(94)00152-9

Solid-State Electronics Vol. 38, No. 3, pp. 661–671, 1995

0038-1101/95 $9.50 + 0.00

VERY-LOW-FREQUENCY (VLF) INVESTIGATIONS OF THE MOSFET'S HIGH-ORDER DERIVATIVES

O. L. YAKYMAKHA[1]† and Y. M. KALNIBOLOTSKIJ[2]

[1]Laboratory of Electron Device Modelling, Department of Electro-Acoustic, 2330, Kyiv Polytechnic Institute, Peremogy Avenue, 37, 252056 Kyiv and [2]1 Biloruska Street, Apt. 5, 252050 Kyiv, Ukraine

(Received 22 January 1994; in revised form 28 May 1994)

Abstract—This paper discusses the generation of the harmonics of the MOSFET as a result of its nonlinear I_d–V_g characteristic in the saturation region at room temperature and higher. The a.c. method presented is based on measuring the high-order derivatives of drain voltage with respect to gate voltage by using a selective amplifier and high pass active filter in the very-low-frequency region. Experimental results show considerable deviation of MOSFET transconductance from a linear dependence on gate voltage in the saturation region, and the resonant type dependences of high-order derivatives on gate and drain voltages at high load resistance values ($R_L > 300\,\Omega$) that can be explained by the simple series resonant circuit model of MOSFETs, and quantum properties of the Si–SiO_2 interface.

1. INTRODUCTION

The present-day approach to the field-effect that takes place in MOSFETs is based on solving Poisson's equation in silicon using Maxwell–Boltzmann[1,2] or Fermi–Dirac[3,4] statistics which give the concentrations of the inversion charges at the Si–SiO_2 interface. At low longitudinal electric fields, Ohm's law has been used:

$$I_d(V) = \mu_0 Z Q_{inv}(dV/dy), \tag{1}$$

where μ_0 is the mean carrier mobility, Z the width of MOSFET and $V(y)$ is the longitudinal potential, in the standard models[5,6]. The inversion charge (Q_{inv}) is found from Kirchhoff's law. At the high values of electric field we should consider the field dependence of mobility[7,8], the simplest phenomenological expression of which is:

$$\mu(V_g) = \mu_0/[1 - \Theta(V_g - V_T)], \tag{2}$$

where Θ is the mobility reduction factor and V_T is the threshold voltage. The physical nature of mobility field dependence has been studied theoretically using different scattering mechanisms[9], but experimental investigations[10,11] have been concerned with mobility as a function of temperature. References [10,12] have shown the equivalence of both a.c. and d.c. techniques for mobility measurements in the frequency range < 100 kHz. Further MOSFET mobility investigations[13,14] have been concerned with improvements of the phenomenological approximation (2) using the Kubo–Greenwood formalism for conductivity at low temperatures (< 77 K).

The latest experimental discovery of periodic inflection in I_d–V_g characteristics ($\Delta V_g = \varphi_g = 1.2$ V)[15] and a resonant frequency dependence of the main MOSFET small-signal parameters in the very-low-frequency (VLF) region[16] requires the quantum mechanical considerations for the MOSFET's conductivity which is due to the surface problem[17] of crystal solids. Since quantum systems have discrete energy levels, the spectroscopic techniques[18], which use the high-order derivative measurements, can be used here too. In the case of plasmon interaction ($\varphi_{ps} \approx \varphi_g = 1.2$ V) between electrons at the Si–SiO_2 interface[16] we shall have a considerable increase of temperatures up to the room values. The effective mass and zone-band approximations are not valid at the Si–SiO_2 interface and electrons (holes) can be considered as free particles again (because their energy is above $\varphi_g = 1.2$ V).

This paper presents the preliminary results of the theoretical and experimental investigations of MOSFET's high-order derivatives of drain current with respect to the gate and drain voltages in the VLF range.

2. EXPERIMENTAL PROCEDURE

Production-type enhancement mode p-channel MOSFETs КП301Б and КП304А were used in this study. The КП301Б has the following values of the internal parameters: $L = 25\,\mu$m (channel length), $Z = 2.2$ mm (channel width), $S_g = (1–2.6)$ mA/V (d.c. transconductance) and $C_{gs} = 3.5$ pF, $C_{gd} = 1$ pF, $C_{ds} = 3.5$ pF are the terminal parasitic capacitances measured at $\nu = 10$ MHz (Ref. [19, p. 578]). The КП304А has the values: $L = 30\,\mu$m, $Z = 4.6$ mm, $S_g = 4$ mA/V and $C_{gs} = 9$ pF, $C_{gd} = 2$ pF, $C_{ds} = 6$ pF

†Address for correspondence: Molodijna Street 34, v. Grygorivka, Obukhiv District, 255406 Kyiv Region, Ukraine.

measured at $\nu = 1$ MHz (Ref. [19, p. 587]). An electric circuit for dynamic measurements is shown in Fig. 1, where the standard selective amplifier (SA) with accuracies about (1–5)% is used for measuring the high-order derivatives of drain current. The digital voltmeters V_1–V_4 can measure the d.c. and a.c. voltages with accuracies about 0.01% (for d.c.) and 0.1% (for a.c.). Load resistors (R_{L1} and R_{L2}) have been chosen to rapidly control the internal MOSFET parameter dependence on load resistance. The selective amplifier has a low selectivity and therefore the high pass active filter (AF) with the cut-off frequency $\nu_F = \omega_F/2\pi = 3.0$ kHz has been used to suppress the main input harmonic when the second, third, etc. derivatives should be measured.

It appears from Appendix A that high-order derivatives are proportional to the a.c. signals measured at fixed frequencies $\omega, 2\omega, 3\omega, \ldots$. Thus, using a fixed input frequency and voltage ($\omega_{in}, v_m = \text{const.}$) applied to the gate terminal we can determine the first derivative by measuring the output a.c. signal, $(V_\sim)_{out}$, (S_2 is switched on and therefore AF is switched off). Actually, when SA is adjusted to the input frequency $\omega_{SA} = \omega_{in}$, we can measure the value

$$(V_\sim)_{out}/(V_\sim)_{in} = (V_\sim)^1/v_m = (dV_d/dV_g), \quad \text{at } \omega_{SA} = \omega_{in} \quad (3a)$$

that is proportional to the first derivative. When SA is adjusted to the second harmonic $\omega_{SA} = 2\omega_{in}$, then we can measure the value

$$(V_\sim)_{out}/(V_\sim)^2_{in} = (V_\sim)^{II}/v_m^2 = (d^2V_d/dV_g^2), \quad \text{at } \omega_{SA} = 2\omega_{in} \quad (3b)$$

that is proportional to the second derivative. The third derivative can be determined at $\omega_{SA} = 3\omega_{in}$, and so on.

Since we have SA with a low selectivity, the AF can be used to measure high-order derivatives (S_2 is switched off in Fig. 1). The a.c. input voltage with fixed amplitude ($v_m = \text{const.}$) and varied frequency ($\omega_{in} = \text{variable}$) is used in that case. When input frequency is equal to the value $\omega_{in} = \omega_{SA}/2$, then SA will measure $(V_\sim)^{II}$ that is proportional to the second derivative. At $\omega_{in} = \omega_{SA}/3$ SA will measure the value $(V_\sim)^{III}$ that is proportional to the third derivative and so on.

It is evident that the simple circuit presented in Fig. 1 allows the possiblity to experimentally determine the a.c. voltages only. In the general case the transition from derivatives of drain voltage dV_d/dV_g, $d^2V_d/dV_g^2, \ldots$ to derivatives of current dI_d/dV_g, $d^2I_d/dV_g^2, \ldots$ is a difficult problem[18]. In any case cumbersome analytical expressions for high-order derivatives can be always obtained and their relation with internal MOSFET's paramters can be calculated by computer technique[18].

3. SURFACE ENERGY LEVELS AND CURRENT–VOLTAGE MOSFET's CHARACTERISTICS

Using the simplest Sah's model[5] we can consider the dependence of mobility on electric field at the Si–SiO_2 interface. For the thermodynamic non-equilibrium the inversion charge can be given in the form

$$Q_{inv}(V) = C_{ox}[V_g - V_T - V(y)]. \quad (4)$$

Inserting eqn (4) into eqn (1) and integrating the result with respect to y over the channel $[O–L]$ we can derive the following equation for the drain current in the saturation region of strong inversion

$$I_d = 0.5\beta_0(V_g - V_T)^2, \quad V_d \geqslant V_{ds} = V_g - V_T \quad (5)$$

where $\beta_0 = \mu_0 C_{ox} Z/L$ is the MOSFET's gain factor, and C_{ox} is the dielectric capacitance[20]. Note that eqn (5) is valid at the low gate voltages only ($V_g < V_{gl}$).

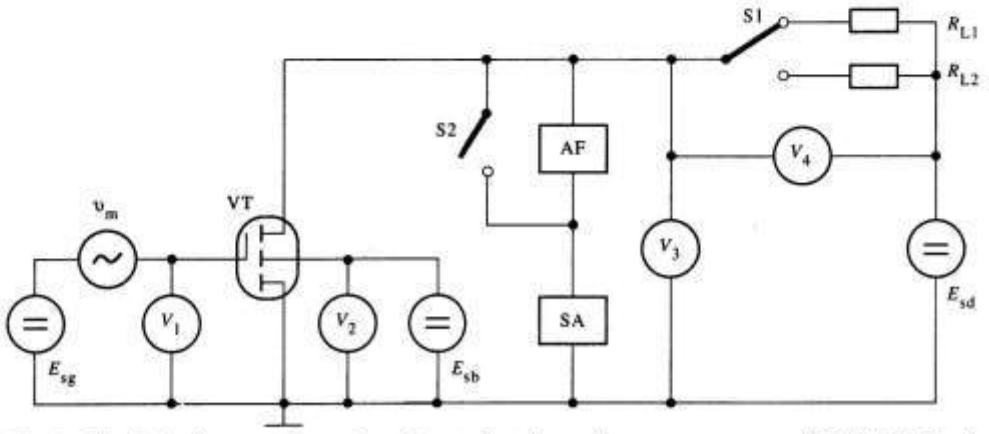

Fig. 1. The block diagram of experimental setup for d.c. and a.c. measurements of MOSFET. Used designations are as follows: VT—transistor; v_m—sound frequency generator; SA—selective amplifier; S1, S2—switches; R_{L1}, R_{L2}—load resistances; E_{sg}, E_{sb} and E_{sd}—regulated supply sources for gate, bulk and drain electrodes respectively; V_1, V_2, V_3 and V_4—digital voltmeters which measure the gate, bulk, drain and load resistor voltage respectively.

In the case of high gate voltage ($V_g \geqslant V_{g1}$) the charge balance law can be rewritten by adding self-compensated charges of opposite signs

$$\pm\Delta Q_{inv} = \pm C_{ox} \times \Delta V_T, \tag{6}$$

that leads to the increase of the total inversion charge

$$Q_{inv\cdot\Sigma} = Q_{inv} + C_{ox}\Delta V_T = C_{ox}[V_g - (V_T - \Delta V_T) - V]. \tag{7}$$

Since experimental data[10] shows a decrease of the MOSFET's gain factor at high gate voltages, we should consider only the γth part of the total charge (7) which takes part in the drain current flow. Substituting γQ_{inv} into eqn (1) the saturation drain current can be expressed as:

$$I_d = 0.5\beta_s[V_g - (V_T - \Delta V_T)]^2, \quad V_g \geqslant V_g - V_T, \tag{8}$$

where $\beta_s = \gamma\beta_0$, γ is the redistribution factor. The additional charges (6), which decrease the threshold voltage $V_T = V_T - \Delta V_T$, are fixed at the $Si-SiO_2$ interface by the surface energy levels. For uniform filling of the energy levels we have, to fulfil the charge balance condition,

$$\Delta Q_{inv} = (1-\gamma)Q_{inv\cdot\Sigma} \tag{9}$$

from which the redistribution factor can be derived at $V = 0$:

$$\gamma = (V_g - V_T)/(V_g - V_T + \Delta V_T). \tag{10}$$

When the condition $\Delta V_T = \Theta(V_g - V_T)^2$ takes place, then eqn (10) can be rewritten in a form the same as the known relationship (2) for the relative mobility ($\mu/\mu_0 = \gamma$) in the strong electric field. Thus, the MOSFET's gain factor can be defined at the high gate voltages as

$$\beta_s = (C_{ox}Z/L) \times \mu_0/[1 + \Theta(V_g - V_T), \quad V_g \geqslant V_{g1}. \tag{11}$$

This approach explains the MOSFET's gain factor decrease by the selfcompensated surface charges of the opposite signs, which are fixed by the surface energy levels (we need minimum two energy levels). But in contrast to the known considerations[7,8] this approach predicts the decrease of the threshold voltage ($V_{T\Sigma} = V_T - \Delta V_T$) too. Furthermore, this approach can be extended on the more complicated case of the 2D electron system with energy levels at the $Si-SiO_2$ interface.

Let us consider formally the case of discrete periodic variation for MOSFET's gain factor with increasing gate voltage in the superstrong inversion regime[21]

$$\beta_{j+1} \leqslant \beta_j; \quad V_{Tj+1} \leqslant V_{Tj}; \quad V_{gj+1} > V_{gj} \tag{12}$$

where $j = 1, 2, 3, \ldots$ are the inflection points of the $I_d - V_g$ characteristic, $\Delta V_{gj} = V_{gj+1} - V_{gj} = \varphi_g = 1.2$ V. The saturation drain current can be given here as:

$$I_{dj} = 0.5\beta_j(V_g - V_{Tj})^2. \tag{13}$$

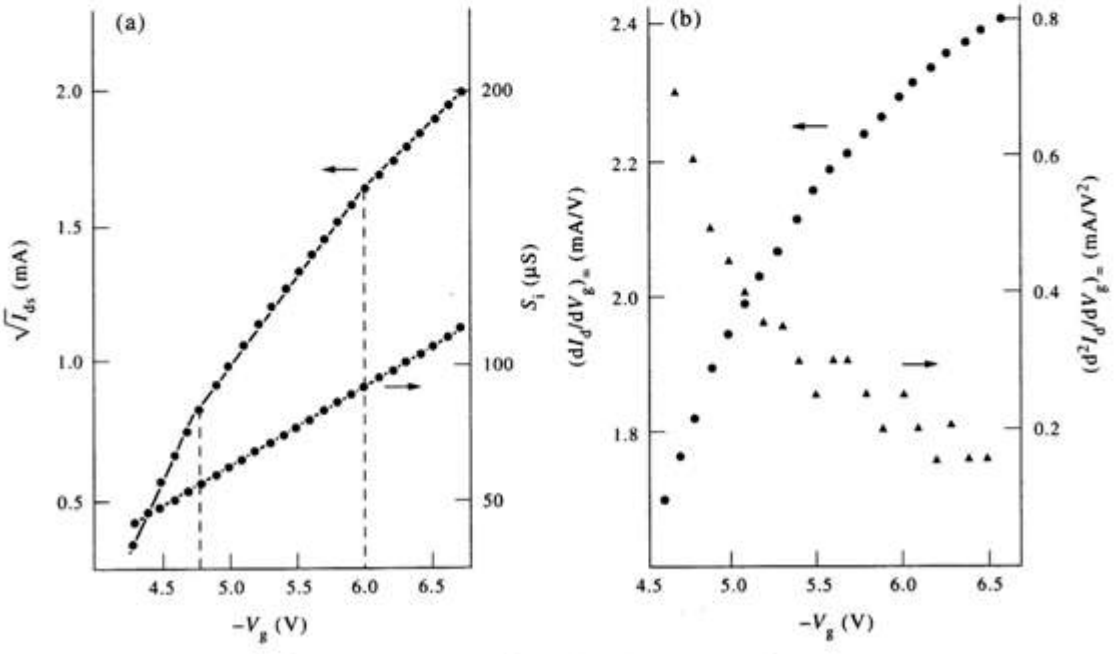

Fig. 2. The d.c. $\sqrt{I_{ds}}$, S_i (a) and dI_d/dV_g, d^2I_d/dV_g^2 (b) dependences on gate voltage for MOSFET КП301Б, N13 at $V_d = -15.0$ V and $T = 293$ K. Used parameters of approximation (13) are as follows: $\beta_1 = 2.10$ mA/V², $V_{T1} = -3.95$ V, $-V_g \leqslant 4.8$ V; $\beta_2 = 0.89$ mA/V², $V_{T2} = -3.50$ V, $4.8\text{ V} < -V_g \leqslant 6.0$ V; $\beta_3 = 0.528$ mA/V², $V_{T3} = -2.80$ V, $6.0\text{ V} < -V_g \leqslant 7.2$ V.

The sets of threshold voltages $\{V_{Tj}\}$ and gate voltages $\{V_{gj}\}$ can be due to the atomic-like complexes at the Si–SiO_2 interface (see Appendix B) with eigenenergy

$$W_j = q(V_{T0} - V_{Tj}) = W_{j_m}/q(j_m - j + 1), \quad (14)$$

where $W_{j_m} = q(V_{T0} - V_{Tj_m}) = 0.5 Z_B W_B$ is the ionization potential, $W_B \approx 6.8$ eV the Bohr energy scale, $Z_B = 1, 2, \ldots$ the atomic number, V_{T0} the ground state threshold voltage that corresponds to the energy of free space, j_m the bound number of inflection points.

The relationship between threshold voltages and gain factors can be given in the form

$$V_{Tj+1} = V_{gj} - (V_{gj} - V_{Tj})\sqrt{\beta_j/\beta_{j+1}} + \sqrt{2/\beta_{j+1}} \times \Delta(\sqrt{I_{dj}}), \quad (15)$$

where $\Delta(\sqrt{I_{dj}}) = \pm(\sqrt{I_{dj+1}} - \sqrt{I_{dj}})$ is the drain current step at the jth inflection point. This equation is valid for the discrete energy levels only. The widening of energy levels can be taken into account by the simple continuous approximation:

$$V_T(V_g) = V_{Tj+1} + (V_{Tj} - V_{Tj+1}) \times \{1 + \cos[V_g - 0.5(V_{gj} + V_{gj+1})]\pi/\varphi_g\}. \quad (16)$$

4. EXPERIMENTAL RESULTS AND DISCUSSION

The simple theoretical model presented in Section 3 considers the saturation drain current only. But MOSFETs have a non zero value of conductance in the saturation region[22]. To extract the differential part of the drain current the following approximation can be used by

$$I_d = I_{ds} + I_{dif}, \quad (17a)$$

where I_{ds} is the saturation drain current which can be approximated by eqn (13) and I_{dif} is the differential part of the drain current which can be approximated as

$$I_{dif} = S_i \times V_d, \quad (17b)$$

where S_i is the saturation conductance.

The typical d.c. dependence of the $\sqrt{I_{ds}}$ on V_g is shown in Fig. 2(a) for КП301Б, N13. The two inflections at $V_{g1} = -4.8$ V and $V_{g2} = -6.0$ V can be seen for this characteristic with different values of β_j and V_{Tj}. Since we measure the drain current at the discrete values of gate voltage with steps equal $\Delta V_{gj} = 0.1$ V, we can calculate the increments as $\Delta I_{dj} = I_{dj+1} - I_{dj}$, $\Delta^2 I_{dj} = \Delta I_{dj+1} - \Delta I_{dj}$, $\Delta V_{gj} = V_{gj+1} - V_{gj}$, from which the high-order d.c. derivatives can be found [$\Delta I_d/\Delta V_g$ and $\Delta^2 I_d/(\Delta V_g)^2$]. The first and second d.c. derivatives for КП301Б, N13 are presented in Fig. 2(b). As can be seen from this figure the first d.c. derivative has a deviation from linear dependence at high gate voltages and therefore the second d.c. derivative decreases monotonically with increasing gate voltage.

Figure 3 shows the results of spectral data processing of КП301Б, N11 for d.c. measurements. This transistor has $j_m = 6$ surface plasmon energy levels at $T = 420$ K which is due to the doping concentration

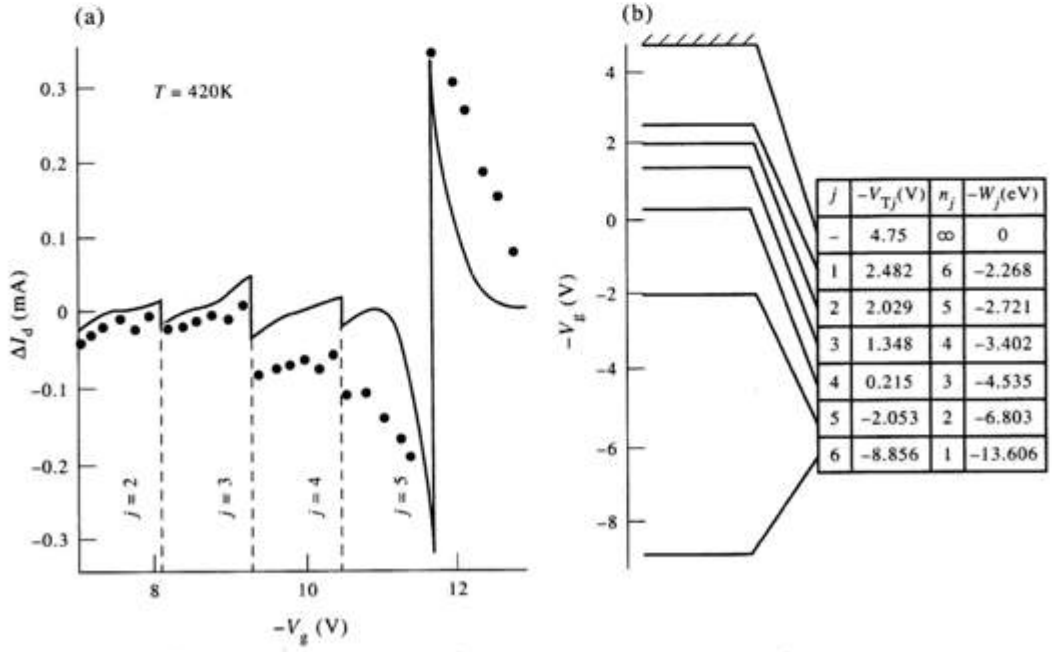

j	$-V_{Tj}$(V)	n_j	$-W_j$(eV)
–	4.75	∞	0
1	2.482	6	–2.268
2	2.029	5	–2.721
3	1.348	4	–3.402
4	0.215	3	–4.535
5	–2.053	2	–6.803
6	–8.856	1	–13.606

Fig. 3. MOSFET N11 of КП301Б type. (a) Static spectral $\Delta I_d - V_g$ characteristics for the first four inflections measured at $V_d = -11$ V and $T = 420$ K. (——) Theoretical approximation (13, 16). (●) Experimental data. (b) Energy levels of MOSFET due to the different values of threshold voltage (V_{Tj}) and gain factor (β_j), where $n_j = j_m - j + 1$.

in substrate. The ionization potential of an atomic-like complex at the $Si-SiO_2$ interface has the value $W_{in} = 13.606$ eV, and therefore $Z_B = 2$. The ground state threshold voltage is $V_{T0} = -4.75$ V. As can be seen from this figure the theoretical approximations (13–16) fit well the experimental data.

First we measure the a.c. high-order derivatives without an active filter. The typical dependences of the first four derivatives on gate voltage are presented in Fig. 4 for КП301Б, N6. As can be seen from Fig. 4(a) the first derivative is practically a linear function in the range $3.7\ \text{V} \leqslant -V_g < 5.0\ \text{V}$. The second derivative has a rapid increase in the range $3.3\ \text{V} \leqslant -V_g \leqslant 4.0\ \text{V}$ (this region can be associated with the weak inversion regime[20]), a maximal value at $-V_g = 4.0$ V (it can be referred to the threshold voltage), and a slow decrease at $-V_g > 4.0$ V (this region can be due to the strong inversion regime). The third derivative has its maximum at $-V_g = 3.65$ V and minimum at $-V_g = 4.0$ V, but the second maximum is not shown because of the low selectivity of the SA.

The physical nature of the maximum of the a.c. second derivative can be explained by the following way. From earlier investigations it is known that transconductance measured in the region below saturation has the inflection point at the dynamic threshold voltage (V_{Tw}) that divides the weak and strong inversion regimes and leads to the nonlinear dependence of mobility on gate voltage (see Figs 45(b), 59, 60 in Ref. [11]). This nonlinear dependence of mobility has been referred to the different scattering mechanisms[11]. We shall use another approach due to the pairs of surface energy levels at the $Si-SiO_2$ interface. Actually, the bell-shaped term can be extracted from the total second derivative $V_\Sigma^{II} = V_b^{II} + V_s^{II}$, where V_b^{II} is the bell-shaped term and V_s^{II} is the strong inversion term of the total second derivative (V_Σ^{II}). The results of this procedure are presented in Fig. 4(b). It is evident that the bell-shaped part of the second derivative can be due to the process of filling the two energy levels by electrons and holes simultaneously. Furthermore, the energy width ($\varphi_g = 1.2$ V) of the bell-shaped

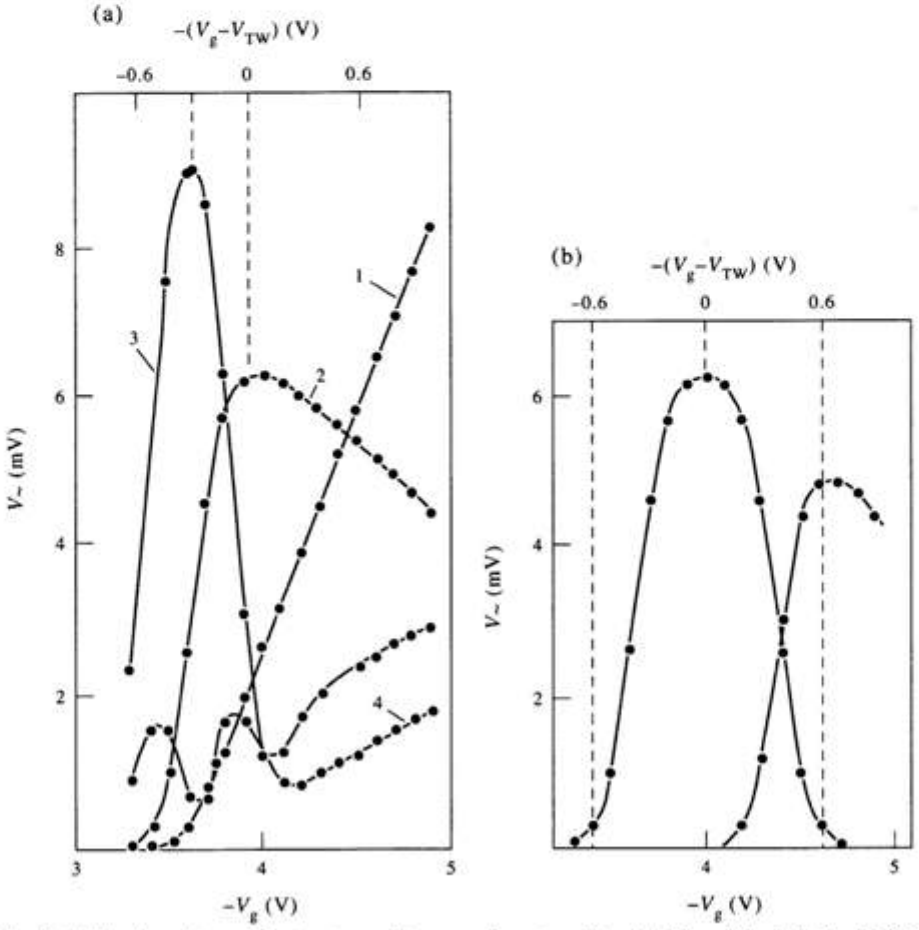

Fig. 4. (a) The dependence of output a.c. voltages on d.c. gate voltage (AF is switched off) for MOSFET КП301Б, N6 at $V_d = -10.0$ V, $T = 293$ K and $R_L = 1.1$ kΩ. Curve 1 is for $(V_\sim)^I$ at $v_m = 6$ mV, $\nu_1 = 2$ kHz. Curve 2 is for $(V_\sim)^{II}$ at $v_m = 90$ mV, $\nu_2 = 1$ kHz. Curve 3 is for $(V_\sim)^{III}$ at $v_m = 280$ mV, $\nu_3 = 0.667$ kHz. Curve 4 is for $(V_\sim)^{IV}$ at $v_m = 280$ mV, $\nu_4 = 0.5$ kHz. (b) The dependence of the modernized second derivative on gate voltage for the same MOSFET with extracted the bell-shaped distribution.

derivative can be due to the energy gap between the two energy levels.

The influences of the magnitude of input signal and load resistance are shown in Fig. 5. Note that an increase of magnitude of input signal from 100 mV [Fig. 5(a)] to 300 mV [Fig. 5(b)] leads to the widening of the bell-shaped distribution on 200 mV for the low value $R_L = 10\,\Omega$ and high $R_L = 1.0\,k\Omega$ values of the load resistance. Furthermore, the value of dynamic threshold voltage (V_{T_0}) is shifting on 100 mV when the magnitude of input signal increases from 100 to 300 mV. Thus, the equivalent widening of the bell shaped part of the second derivative can be due to the widening of the discrete energy level caused by the high magnitude of the input signal.

An improvement of the measuring process at the high values of gate voltage can be achieved by using the active filter. Figure 6 shows the typical dependence of the second, third and fourth a.c. derivatives on gate voltage. We can see in Fig. 6(a) some improvements for the third derivative only, since it receives the second maximum at $-V_g = 4.1$ V. The number of maxima for the fourth derivatives is not changed. These phenomena can be explained by the mono-polar conductivity of the MOSFETs. The point is that the pair of energy levels is being filled by the selfcompensated electrons and holes in the latent form (it causes the shifting of the threshold voltage), but the drain current is formed by the holes or electrons only. Therefore we shall have only one-half of the distribution function that shows the widening of the energy levels. But the most intriguing phenomena is shown in Fig. 6(b) in the range $7.0\,V \leqslant -V_g \leqslant 8.4\,V$. Note that all measured derivatives show the resonant type dependence the nature of which will be considered below.

As can be seen from Fig. 7 the first derivative is a piecewise linear function of gate voltage with period about ~ 1.2 V. Its slope decreases with increasing gate voltage. Since the curves 2 and 3 have the same values of voltage transmission factor over the entire range of gate voltages, it gives the evidence to support the validity of the measuring process. The comparison of the d.c. and a.c. first derivatives shows that the inflection points are shifted on 300 mV (see Fig. 7). Note that these points are independent of magnitude of input signal.

Figure 8 shows the dependence of a.c. first derivative on d.c. gate voltage at different values of load resistance and a.c. input voltage. As can be seen from this figure the first derivative measured at the low value of load resistance ($R_L = 10\Omega$) does not show the resonant phenomena in the gate voltage range $4.0\,V \leqslant -V_g \leqslant 9.0\,V$. Furthermore, the inflection

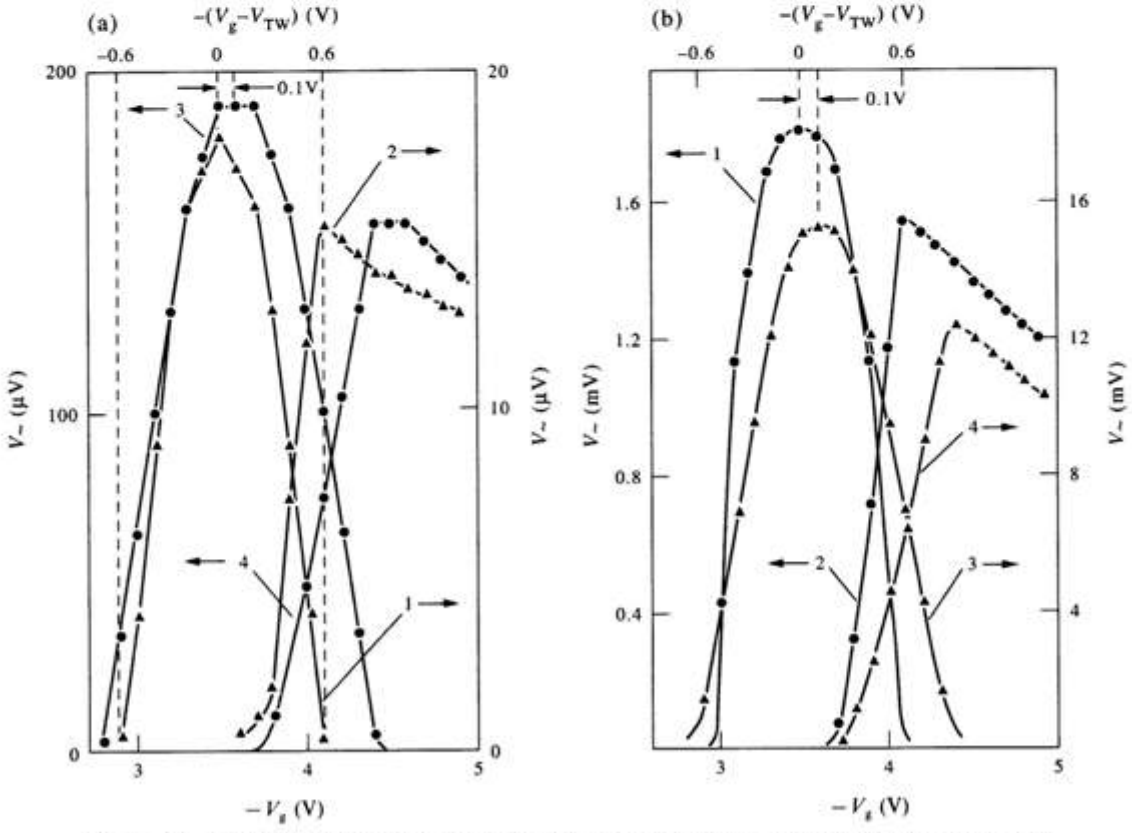

Fig. 5. The dependence of modernized second derivative on gate voltage (AF is switched on) with extracted the bell-shaped distribution for MOSFET КП301Б, N11 measured at $V_d = -15.0$ V, $T = 293$ K, $\nu_2 = 1.5$ kHz and $R_L = 10\,\Omega$ (a). The same dependence measured at $R_L = 1.0\,k\Omega$ (b). Curves 1,2: $v_m = 100$ mV. Curves 3, 4: $v_m = 200$ mV.

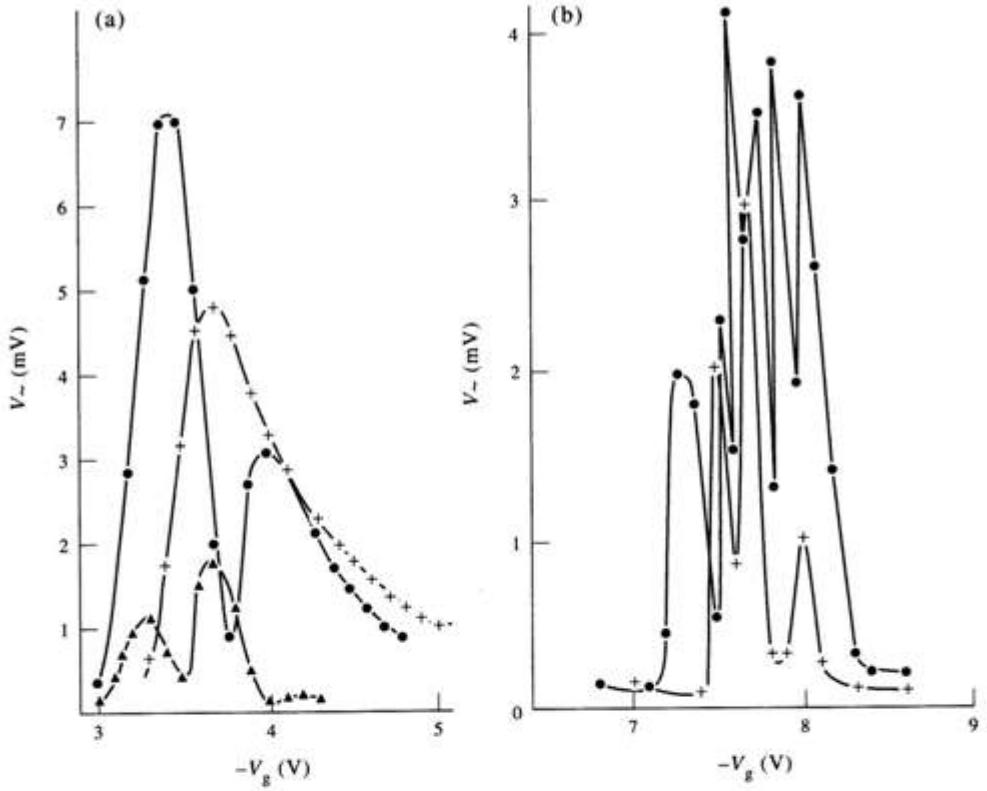

Fig. 6. The typical dependence of output a.c. voltage on d.c. low (a) and high (b) gate voltage (selective amplifier is adjusted on fixed frequency $\nu_{SA} = 3.0$ kHz and AF is switched on). for MOSFET КП301Б, N3 measured at $V_d = -15.0$ V, $T = 293$ K and $R_L = 1.1$ kΩ. ×—$(V_{\sim})^{II}$ is measured at $v_m = 100$ mV and $\nu_{in} = 1.5$ kHz. ●—$(V_{\sim})^{III}$ is measured at $v_m = 300$ mV and $\nu_{in} = 1.0$ kHz. ▲—$(V_{\sim})^{IV}$ is measured at $v_m = 300$ mV and $\nu_{in} = 0.75$ kHz.

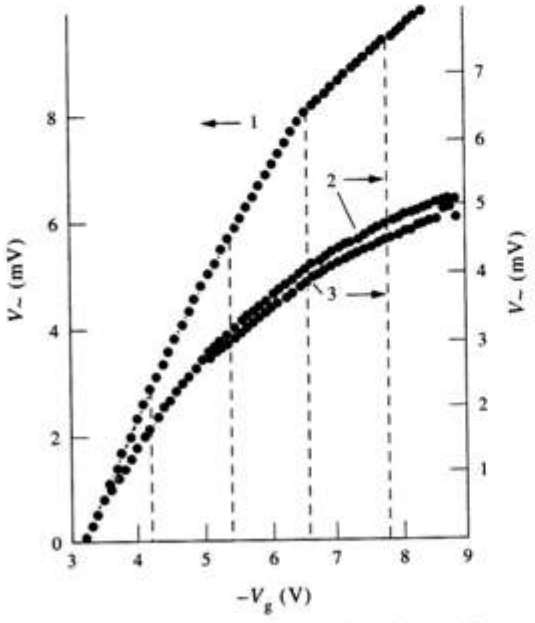

Fig. 7. The dependence of first a.c. derivative on d.c. gate voltage for КП301Б, N11 measured at $V_d = -15.0$ V, $T = 293$ K, $\nu_1 = 3.0$ kHz and $R_L = 1.0$ kΩ and different values of input signal. Curve 1: $v_m = 6.5$ mV, $V_{\sim}$ has the scale × 1 mV. Curve 2: $v_m = 300$ mV, $V_{\sim}$ has the scale × 100 mV. Curve 3: $v_m = 30$ mV, $V_{\sim}$ has the scale × 10 mV.

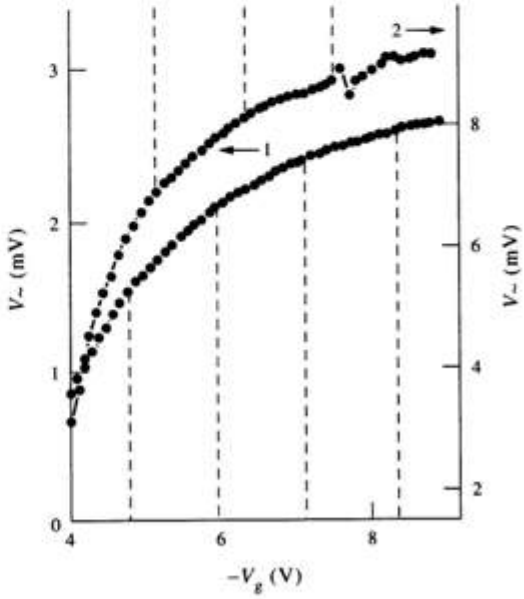

Fig. 8. The dependence of first a.c. derivative on d.c. gate voltage for КП301Б, N3 measured at $V_d = -15.0$ V, $T = 293$ K and different values of load resistance and input signals. Curve 1: $v_m = 100$ mV, $R_L = 10\,\Omega$, $\nu_1 = 1.6$ kHz. Curve 2: $v_m = 5$ mV, $R_L = 1.1$ kΩ, $\nu_1 = 3.0$ kHz.

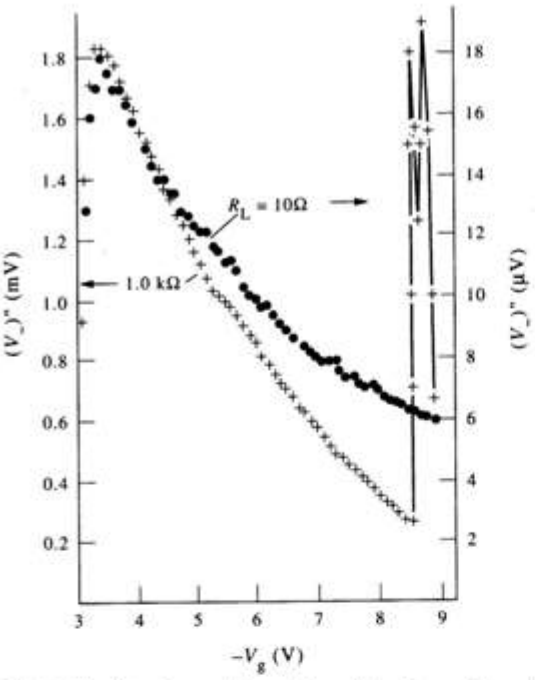

Fig. 9. The dependence of second a.c. derivative on d.c. gate voltage for КП301Б, N11 measured at $V_d = -15.0$ V, $T = 293$ K, $v_m = 100$ mV, $\nu_2 = 1.5$ kHz and different values of load resistance. Curve 1: $R_L = 10\,\Omega$. Curve 2: $R_L = 1.0$ kΩ.

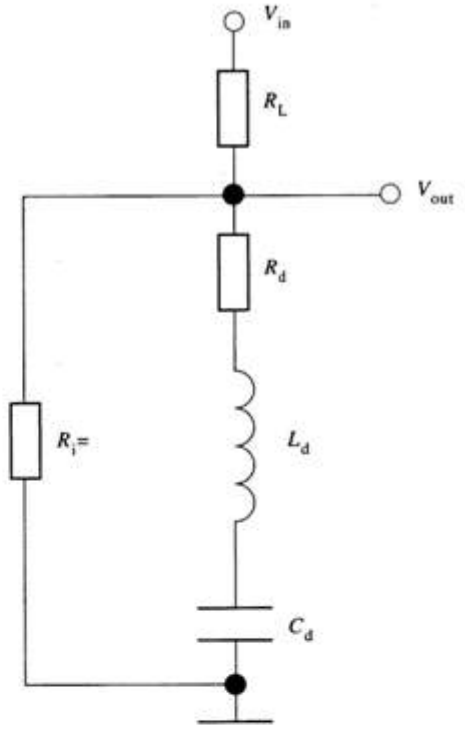

Fig. 10. Equivalent series resonant circuit for frequency dependent MOSFET's amplifier parameters in the case of common-source connection.

points in that case are the same as those in the d.c. case shown in Fig. 3(a). But for the high value of load resistance ($R_L = 1.1$ kΩ) the a.c. first derivative has the resonant phenomena at $-V_g = 7.7$ V and its inflection points are shifted on 400 mV with respect to the d.c. case. Thus, the main factor that influences on the a.c. measurements is the value of load resistance.

Figure 9 shows the dependence of a.c. second derivative on d.c. gate voltage for different values of load resistance. As can be seen from this figure the second derivative decreases monotonically with increasing d.c. gate voltage. Moreover, the resonant phenomena take place for $R_L = 1.0$ kΩ only at $-V_g \geqslant 8.6$ V. The data presented are valid since the correlation of the second derivatives

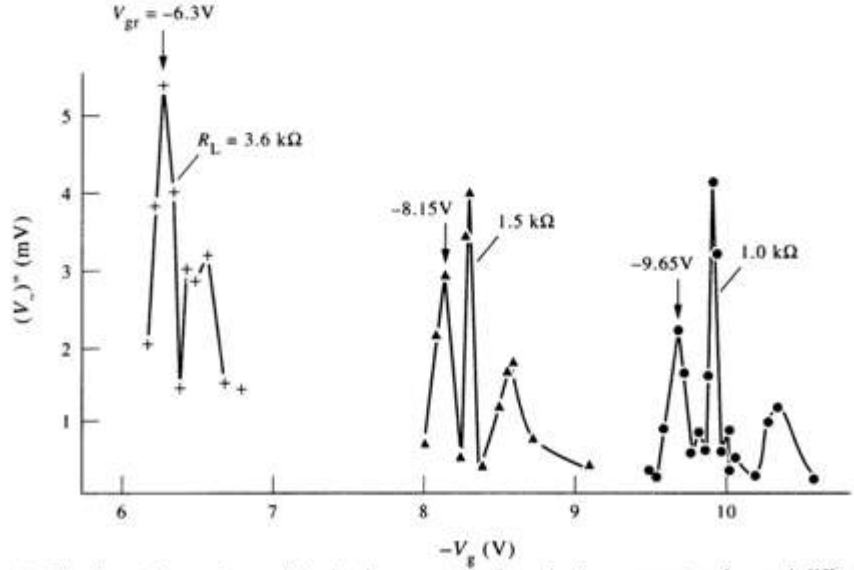

Fig. 11. The dependence of second derivative on gate voltage in the resonant region and different load resistances. Curve 1: $R_L = 1.0$ kΩ. Curve 2: $R_L = 1.5$ kΩ. Curve 3: $R_L = 3.6$ kΩ.

$V^{II}(R_{L1})/V^{II}(R_{L2})$ is approximately equal to the correlation of load resistance $R_{L1}/R_{L2} = 10\,\Omega/1000\,\Omega$. The lack of the stepped variation of the second derivative could be referred to the widening of the energy levels. The simple equivalent series resonant circuit shown in Fig. 10 may be used to explain the frequency dependence of the MOSFET's amplifier parameters. This circuit is based on the model presented in Ref. [16]. It's resonant function can be given as

$$F(\omega) = K_v(\omega_d)/|\dot{K}_v(\omega)| \approx \{1 + Q_\Sigma^2(\omega/\omega_d - \omega_d/\omega)^2\}^{-1/2}, \quad (18a)$$

where

$$Q_\Sigma = (\omega_d L_d/R_d)\sqrt{1 + 2R_d/R_L} \quad (18b)$$

is the quality factor of LC-circuit, $\omega_d = \sqrt{L_d C_d}$ the resonant frquency, and $\dot{K}_v(\omega)$ is the voltage transmission factor.

In our earlier work[16], it has been shown that the internal parameters of MOSFETs are frequency dependent; caused by quantum Schottky effect at the

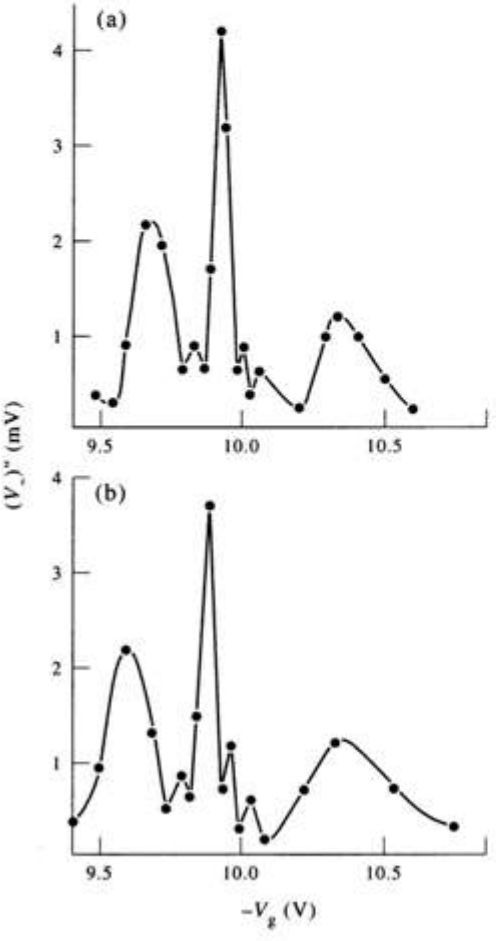

Fig. 12. The dependence of second derivative on gate voltage in the resonant region at $V_d = -20$ V (a) and at $V_d = -40$ V (b) for КП301Б, N11 with $v_m = 100$ mV and $R_L = 1.0$ kΩ.

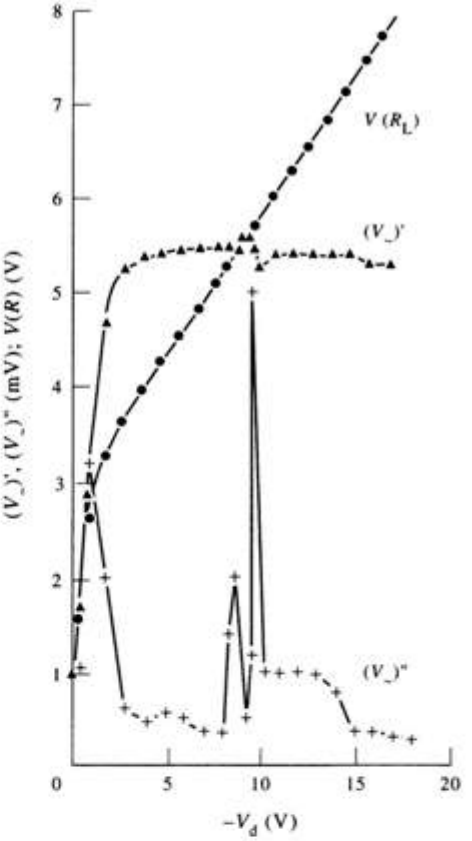

Fig. 13. The dependence of d.c. and a.c. output voltages on d.c. drain voltage for КП304А, N4 measured at $v_{SA} = 3.0$ kHz, $T = 293$ K, $V_g = -6.2$ V and $R_L = 1106\,\Omega$. Curve 1: static voltage drop $V(R_L)$ across the load resistor R_L is determined at $V_b = 0$. Curve 2: first derivative $(V_\sim)'$ is determined at $v^m = 10$ mV and $v_m = 3.0$ kHz. Curve 3: second derivative $(V_\sim)''$ is determined at $v_m = 300$ mV and $v_m = 1.5$ kHz.

Si–SiO_2 interface. The Schottky capacitance C_d and inductance L_d are functions of gate voltage and temperature. Furthermore, they have the bound values $C_0 = 5.216 \times 10^{-7}$ F, and $L_0 = 7.407 \times 10^{-2}$ H with characteristic impedance about the wave vacuum value $\rho_0 = \sqrt{L_0/C_0} = 376.73\,\Omega$. Therefore, at the low values of the load resistance ($R_L < 300\,\Omega$) the a.c. derivatives of drain current will be the same as those for the d.c. ones. In the case when the load resistance has the value about characteristic impedance of the RLC circuit, then we shall have the resonant type dependence of the a.c. derivatives at high gate voltages. It is evident that the resonant value of gate voltage decreases with increasing load resistance (see Figs 8 and 9, where resonances are shown only for curves measured at $R_L = 1.1$ kΩ in the range $4\text{ V} \leqslant -V_g \leqslant 9\text{ V}$). Figure 11 shows the dependence of the second derivative on gate voltage for three values of the load resistance in the resonant gate voltage range. From this figure we observe that an increase of the load resistance causes a corresponding decrease of the threshold resonant voltage (V_{TR}). For instance, $-V_{TR} = 9.65$ V for $R_L = 1.0$ kΩ and

$-V_{TR} = 6.3$ V for $R_L = 3.6\,k\Omega$. Note that the threshold resonant voltage is practically constant ($-V_{TR} = 9.91$ V) in the wide range of drain voltages $10\text{ V} \leqslant -V_d \leqslant 40\text{ V}$ (see Fig. 12) for $R_L = \text{const}$.

The resonant properties of the high-order derivatives considered above for I_d–V_g characteristics can be observed in I_d–V_d characteristics too. The typical experimental resonant structure for the first two derivatives and drain current $V(R_L) = I_d R_L$ dependence on drain voltage is shown in Fig. 13 for КП304А, N4 when the sound generator is placed in the drain circuit. From this figure one may observe two regions. The triode region is characterized by the sharp increase of drain current and first derivative at $-V_d \leqslant 3.0$ V. In the saturation region at $-V_d > 3.0$ V the drain current slowly increases with increasing drain voltage and therefore the first derivative is almost constant. The resonance caused by the reactive parameters of MOSFET can be observed in the range $8\text{ V} < -V_d < 10\text{ V}$. The most brightly resonant picture may be seen for the second derivative $(V_\sim)^{11}$.

5. CONCLUSION

The results presented in this paper may be summarized in the following way.

It is found experimentally that MOSFET transconductance shows the considerable deviation from linear dependence on gate voltage in the saturation region. The first resonant structure of the a.c. high-order derivatives takes place at the low gate voltage region and can be due to the process of filling the two surface energy levels with $\Delta\varphi = \varphi_2 - \varphi_1 = \varphi_g = 1.2$ V. The second resonant structure of the a.c. high-order derivatives takes place at the high gate voltage region and can be due to the quantum Schottky capacitance (C_d) and inductance (L_d) at the Si–SiO_2 interface. The periodic ($\Delta V_g = 1.2$ V) structure of the first a.c. derivative has the same inflection points as the direct drain current does at the low values of load resistance $R_L < 300\,\Omega$, but a displacement is observed at $R_L > 300\,\Omega$.

REFERENCES

1. R. H. Kingston and S. F. Neustadter, *J. appl. Phys.* **26,** 718 (1955).
2. B. E. Deal, A. S. Grove, C. T. Sah and E. H. Snow, *Solid-St. Electron.* **8,** 145 (1965).
3. R. Seiwatz and M. Green, *J. appl. Phys.* **29,** 1034 (1958).
4. T. I. Kamins and R. S. Muller, *Solid-St. Electron.* **10,** 423 (1967).
5. C. T. Sah, *IEEE Trans. Electron Devices* **ED-11,** 324 (1964).
6. C. T. Sah and H. C. Pao, *IEEE Trans. Electron Devices* **ED-13,** 393 (1966).
7. O. Leistiko, A. S. Grove and C. T. Sah, *IEEE Trans. Electron Devices* **12,** 248 (1965).
8. R. H. Crawford, *MOSFET in Circuit Design*, p. 182. McGraw-Hill, New York (1967).
9. C. T. Sah, T. H. Ning and L. L. Tschopp, *Surface Sci.* **32,** 561 (1972).
10. F. F. Fang and A. B. Fowler, *Phys. Rev.* **13,** 619 (1968).
11. T. Ando, A. Fowler and F. Stern, *Rev. mod. Phys.* **54,** N2 (1982).
12. P. J. T. Mellor, *Proc. IEE* **118,** 1393 (1971).
13. G. Gibaudo, *Solid-St. Electron.* **32,** 87 (1989).
14. G. Gibaudo and F. Balestra, *Solid-St. Electron.* **32,** 221 (1989).
15. O. L. Yakymakha, *High Temperature Quantum Galvanomagnetic Effects in Two-Dimensional MOSFET Inversion Layers*, p. 91. Vyscha Shkola, Kyiv (1989) (in Russian).
16. O. L. Yakymakha and Y. M. Kalnibolotskij, *Solid-St. Electron.* **37,** 1739 (1994).
17. A. Zangwill, *Physics at Surfaces*. Cambridge Univ. Press, New York (1988) (Russian edn, 1990).
18. E. L. Volf, *Principles of Electron Tunnelling Spectroscopy*. Oxford Univ. Press, New York (1985) (Ukrainian edn, 1990).
19. *The Most Commonly Used Soviet Transistors* (Edited by B. L. Perelman *et al.*), p. 656. Radio i Svyaz, Moscow (1981) (in Russian).
20. S. M. Sze, *Physics of Semiconductor Devices*, 2nd edn, p. 355. Wiley–Interscience, New York (1981).
21. Y. M. Kalnibolotskij and O. L. Yakymakha, Asymptotic MOSFET scaling model. *Proc. 4th Mideuropean Conf. on Custom-Application Specific Integrated Circuits*, Budapest (19–23 May 1993).
22. V. K. G. Reddi and C. T. Sah, *IEEE Trans. Electron Devices* **ED-12,** 139 (1965).
23. G. Arfken, *Mathematical Method for Physicist*, Academic Press, New York. Russian edn, p. 712, Atomizdat, Moscow (1970).

APPENDIX A

Principles of Spectroscopic Investigations

Generally, the idea of spectroscopic investigations is based on determination of the high-order derivatives for the piecewise function. In the case of linear piecewise function [see Fig. A1(a)] its first derivative will be a stepped function [Fig. A1(b)] and its second derivative will be a bell-shaped function [Fig. A1(c)] near the point of inflection. Some extension of the functions in Fig. 1 near the inflection point is caused by non-zero temperature ($T \gg 0$). Experimental determination of derivatives from drain current can be made using a.c. small signal

$$(V_\sim)_{in} = v_m \cos \omega t \tag{A1}$$

applied to the gate terminal with its amplitude (v_m) considerably less than the potential gap in the silicon ($v_m \ll \varphi_g$).

Functional dependence of drain current on gate voltage may be formally expanded in a Taylor series near the operation point V_g[3]:

$$\begin{aligned} I_d[V_g + (V_\sim)] \approx{}& I_d(V_g) + (dI_d/dV_g)(V_\sim) \\ &+ (d^2I_d/dV_g^2)(2!)^{-1}(V_\sim)^2 \\ &+ (d^3I_d/dV_g^3)(3!)^{-1}(V_\sim)^3 + \cdots . \end{aligned} \tag{A2}$$

Considering the known trigonometric expressions

$$\begin{aligned} \cos^2 \omega t &= (1 + \cos 2\omega t)/2, \\ \cos^3 \omega t &= (\cos 3\omega t + 3 \cos \omega t)/4 \end{aligned} \tag{A3}$$

we can rewrite eqn (A2) in the form

$$\begin{aligned} I_d(V_g + v_m \cos \omega t) \approx{}& I_d(V_g) + (dI_d/dV_g)v_m \cos \omega t \\ &+ (d^2I_d/dV_g^2)v_m^2(1 + \cos 2\omega t)/4 \\ &+ (d^3I_d/dV_g^3)v_m^3(3 \cos \omega t + \cos 3\omega t) \\ &/24 + \cdots . \end{aligned} \tag{A4}$$

Using a standard selective amplifier adjusted step-by-step on frequencies $\omega, 2\omega, 3\omega, \ldots$ we can measure a.c. output signals which correspond to the first, second, third, etc. derivatives.

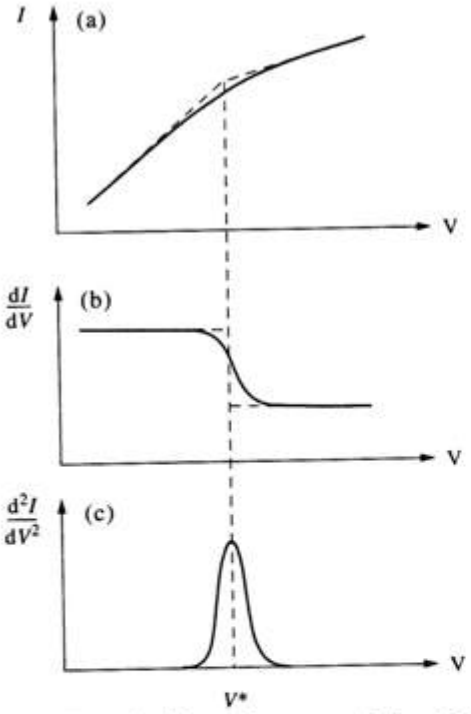

Fig. A1. The main ideas of spectroscopic investigation which considers measurements of minimum three type characteristics: $I - V$ (a), $dI/dV - V$ (b) and $d^2I/dV^2 - V$ (c) for one inflection at $V = V^*$.

APPENDIX B

Atomic-like Complexes at the Si–SiO_2 Interface

Let us formally consider the radial part of the Schrodinger's equation for the atomic problem[23]

$$-(\hbar^2/2m^*r^2)(d^2/dr^2)[r^2(dR/dr)] + U(r)R - WR = 0, \quad \text{(B1)}$$

where the potential energy can be chosen as a probe function

$$U(r) = U_0(r) \times (W_B^*/W)^{|\kappa-1|/2} \quad \text{(B2)}$$

and $W_B^* = 0.5\alpha^2 m^* c^2 = 6.803$ eV is the Bohr energy scale, $-U_0(r) = Z_B q^2/4\pi\epsilon_0 r$ is the Coulomb potential energy, Z_B the atomic number, and

$$m^* = m_n m_p/(m_n + m_p) = 0.5m \quad \text{for} \quad m_n = m_p = m, \quad \text{(B3)}$$

κ is the screening parameter for Coulomb interaction (other designations are the same as usual).

Using the following designations:

$$\rho = \eta r, \quad \lambda = 2mq^2 Z_B^{1/\kappa}/(4\pi\epsilon_0 \hbar^2 \eta),$$

$$\eta^2 = -8mW/\hbar^2 \quad (W < 0) \quad \text{(B4)}$$

the Schrodinger eqn (B1) can be rewritten in the form of Leguerre's equation

$$\rho^{-2}(d/d\rho)[\rho^2(dR/d\rho)] + [\lambda^\kappa/\rho - 1/4 - L(L+1)/\rho^2]R = 0. \quad \text{(B5)}$$

where L is the orbital number. Note that the values λ^κ in eqn (B5) should be integer

$$\lambda^\kappa = Z_B[2mq^2/4\pi\epsilon_0\hbar^2\eta] = n = 1, 2, 3, \ldots. \quad \text{(B6)}$$

Thus, from restriction (B6) the eigenenergy can be derived

$$W_n(\kappa) = -(W_B/2)(Z_B/n)^{2/\kappa}. \quad \text{(B7)}$$

In the case of three-dimensional (3D) system the screening parameter will be $\kappa = 1$, and eigenenergy (B7) will be the same as for the standard Bohr atom[23]. However, in the case of four-dimensional (4D) system it will be $\kappa = 2$ and eigenenergy (B7) can be rewritten as:

$$W_n(\kappa = 2) = -(W_B^*/2)(Z_B/n). \quad \text{(B8)}$$

This equation is equivalent to the experimental approximation (14).